ACS APPLIED MATERIALS & INTERFACES

Research Article

www.acsami.org

D-A-π-A Featured Sensitizers Bearing Phthalimide and Benzotriazole as Auxiliary Acceptor: Effect on Absorption and Charge Recombination Dynamics in Dye-Sensitized Solar Cells

Wenqin Li, Yongzhen Wu, Qiong Zhang, He Tian, and Weihong Zhu*

Shanghai Key Laboratory of Functional Materials Chemistry, Key Laboratory for Advanced Materials and Institute of Fine Chemicals, East China University of Science and Technology, Shanghai 200237, P. R. China

Supporting Information

ABSTRACT: Two organic D-A-π-A sensitizers **LS-2** and **WS-5** containing *N*-octyl substituted phthalimide and benzotriazole as auxiliary electron withdrawing units with similar dimension and structure architecture were systematically studied, focusing on photophysical and electrochemical as well as photovoltaic properties in nanocrystalline TiO_2-based dye-sensitized solar cells (DSSCs). Interestingly, with similar five-member benzo-heterocycles, the two auxiliary acceptors of phthalimide and benzotriazole play exactly different roles in absorption and intramolecular charge transfer: (i) in contrast with **WS-5** delocalized throughout the entire chromophore, the HOMO orbital of **LS-2** is mainly located at the donor part due to the twist conformation with the existence of two carbonyl groups in phthalimide; (ii) the dihedral angles of "D-A" plane and "A-π" plane in **LS-2** further suggest that the incorporation of phthalimide moiety results in curvature of electron delocalization over the whole molecule, in agreement with its blue-shifted, relatively narrow absorption spectra and low photocurrent density; (iii) in contrast with the beneficial charge transfer of benzotriazole in **WS-5**, the phthalimide unit in **LS-2** plays an oppositely negative contribution to the charge transfer, that is, blocking intramolecular electron transfer (ICT) from donor to acceptor to some extent; and (iv) in electrochemical impedance spectroscopy, the incorporated benzotriazole unit enhances electron lifetime by 18.6-fold, the phthalimide only increases electron lifetime by 5.0-fold. Without coadsorption of chenodeoxylic acid (CDCA), the DSSCs based on **WS-5** exhibited a promising maximum conversion efficiency (η) of 8.38% with significant enhancement in all photovoltaic parameters (J_{SC} = 15.79 mA cm^{-2}, V_{OC} = 791 mV, ff = 0.67). In contrast, with the very similar D-A-π-A feature changing the additional acceptor from benzotriazole to phthalimide unit, the photovoltaic efficiency based on **LS-2** was only 5.11%, decreased by 39%, with less efficient photovoltaic parameters (J_{SC} = 10.06 mA cm^{-2}, V_{OC} = 748 mV, ff = 0.68). Therefore, our results demonstrate that it is essential to choose proper subsidiary withdrawing unit in D-A-π-A sensitizer configuration for DSSCs.

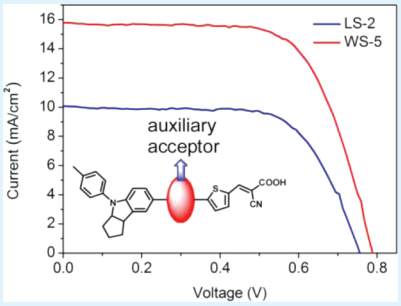

KEYWORDS: *D-A-π-A, solar cells, phthalimide, benzotriazole, absorption, charge recombination*

INTRODUCTION

Along with increasing energy demands and global warming problems, dye-sensitized solar cells (DSSCs) are considered as promising candidates for cheap and sustainable energy sources due to their facile structural modifications, low cost, and environmentally friendly nature.[1] Up to now, DSSCs based on zinc porphyrin dye have been reported with a high photoelectric conversion yield (η) exceeding 12.0% under standard AM 1.5 sunlight irradiation.[2] As a vital component, the sensitizer has the function of absorbing light and injecting electrons into the conduction band of TiO_2 films, while the redox couples in electrolyte play an important role in fast reduction of dye cations. Therefore, it is crucial that the HOMO and LUMO energy of sensitizers should match the corresponding conduction band energy level (E_{CB}) of TiO_2 and the redox potential of oxide species I^-/I_3^-.[3] Recently, donor-π-acceptor (D-π-A) configuration for metal free organic sensitizers has been widely used due to feasible modification in enhancing light-harvesting ability and adjusting HOMO and LUMO levels.[4] On the basis of this model, we further put forward a new configuration defined as D-A-π-A, which introduces an auxiliary acceptor between the donor and π bridge to further promote ICT process.[5] Our previous work has also demonstrated that the incorporation of an additional acceptor is beneficial to dye stability due to effectively dispersing the lone pair electrons of nitrogen in the indoline unit.[5,6a] Efficient light-harvesting, electron injection, and hindrance of charge recombination are critical factors corresponding to the two crucial parameters of photocurrent density (J_{SC}) and open-circuit voltage (V_{OC}) in DSSCs.[7] Co-adsorption of chenodeoxycholic acid (CDCA) with steric structure can inhibit unfavorable dye aggregation and facilitate electron injection, thus realizing the enhancement of J_{SC}.[8] However, a large amount of CDCA has been proved to leave

Received: January 19, 2012
Accepted: March 2, 2012
Published: March 2, 2012

   dx.doi.org/10.1021/am3001049 | *ACS Appl. Mater. Interfaces* 2012, 4, 1822–1830

protons on the TiO_2 and decrease the conduction band edge, resulting in a loss in V_{OC}.[9] Besides, the introduction of CDCA always occupies TiO_2 sites and decreases the dye coverage, which potentially limits further improvement in the photovoltaic performance.[1c] Structure modification with incorporation of a long alkyl is a rational strategy to balance both V_{OC} and J_{SC}.

Phthalimide[10] and benzotriazole[11] derivatives have been vigorously investigated in organic photovoltaics, organic thin film transistors, and organic light emitting diodes due to their good electron affinity and easy solubility modification by introducing a long alkyl chain to the nitrogen site. It is worth mentioning that both phthalimide and benzotriazole are five-member benzo-heterocycles with similar dimension and structure architecture. Up to now, an insight into the selection of proper additional unit in the D-A-π-A configuration has seldom been involved. Accordingly, herein, we incorporated phthalimide and benzotriazole into the D-A-π-A configuration to design sensitizers **LS-2** and **WS-5** and systematically investgated their absorption spectra and electrochemical and photovoltaic properties. **LS-1** with traditional D-π-A configuration was introduced as reference dye. Interestingly, we found that with the very similar structure, the two D-A-π-A dyes **LS-2** and **WS-5** show distinctly different variations in absorption spectra and electrochemical property. The molecular simulation indicates that the HOMO orbital for **WS-5** has a π orbital delocalization throughout the entire molecule, while for **LS-2** it is mainly localized at the donor part with phthalimide as auxiliary acceptor. The existence of carbonyl groups in phthalimide may interrupt the rotation of aryl groups resulting in large dihedral angles of "D-A" planes and "A-π" planes, which is unfavorable to electron delocalization throughout the whole structure and transition from the donor part to acceptor. DSSCs sensitized with **LS-2** and **WS-5** show distinctly different performances in both photocurrent and photoelectric conversion yield. Our results indicate that the introduction of auxiliary electron withdrawing unit in the D-A-π-A configuration should be carried out carefully.

EXPERIMENTAL SECTION

Materials. Unless otherwise stated, starting materials were used as commercially purchased and without any further purification. Tetrahydrofuran (THF) was predried over 4 Å molecular sieves and distilled under argon atmosphere from sodium benzophenone ketyl immediately prior to use. The intermediate of *N*-octylphthalimide was synthesized according to the corresponding literature.[10a] All aldehyde intermediates were synthesized by conventional Suzuki cross-coupling reaction with a relatively high yield, followed by Knoevenagel reaction to get the final sensitizers. Synthesis of **WS-5** was reported previously.[5b]

Characterization. ^{1}H NMR and ^{13}C NMR spectra were recorded on a Bruker AM 400 spectrometer with tetramethylsilane (TMS) as the internal standard, operating at 400 and 100 MHz, respectively. HRMS were recorded with a Waters ESI mass spectroscopy. The UV–vis spectra were measured with a model CARY 100 spectrophotometer. The cyclic voltammograms of the dyes were obtained with a Versastat II electrochemical workstation (Princeton Applied Research) using a three-electrode cell with a Pt working electrode, a Pt wire auxiliary electrode, and a saturated calomel reference electrode (SCE) in saturated KCl solution; 0.1 M tetrabutylammonium hexafluorophosphate ($TBAPF_6$) was used as the supporting electrolyte in CH_2Cl_2. The scan rate was 100 mV s^{-1}.

Synthesis of 2. Bromo-substituted indoline **1** (500 mg, 1.52 mmol), 5-formylthiophen-2-yl boronic acid (261 mg, 1.67 mmol), K_2CO_3 (2 M, 15 mL), and $Pd(PPh_3)_4$ (30 mg, 0.03 mmol) were dissolved in 30 mL of THF, and the mixture was heated to 80–90 °C under a nitrogen atmosphere to reflux for 12 h. After cooling to room temperature, the mixture was extracted with CH_2Cl_2 (50 mL × 3). The organic portion was combined and removed by rotary evaporation. The residue was purified by column chromatography using silica gel (CH_2Cl_2/petroleum ether = 5/1) to give a yellow solid of 223 mg (Yield 41%). ^{1}H NMR (400 MHz, $CDCl_3$, ppm): δ 9.82 (s, 1H), 7.67 (d, J = 4.0 Hz, 1H), 7.40 (s, 1H), 7.37 (dd, J = 8.4 Hz, 1.6 Hz, 1H), 7.23 (d, J = 4.4 Hz, 1H), 7.18 (m, 4H), 6.83 (d, J = 8.0 Hz, 1H), 4.84 (m, 1H), 3.85 (m, 1H), 2.35 (s, 3H), 2.08 (m, 1H), 1.91 (m, 2H), 1.78 (m, 1H), 1.70 (m, 1H), 1.55 (m, 1H). ^{13}C NMR (100 MHz, $CDCl_3$, ppm): δ 182.40, 156.25, 149.67, 139.96, 139.51, 138.02, 135.82, 132.51, 129.92, 126.42, 122.98, 122.84, 121.49, 120.89, 107.25, 69.48, 45.15, 35.21, 33.53, 24.37, 20.84. HRMS (ESI, m/z): $[M + H]^+$ calcd for $C_{23}H_{22}NOS$, 360.1422; found, 360.1423.

Synthesis of LS-1. Intermediate **2** (105 mg, 0.29 mmol) and cyanoacetic acid (248.4 mg, 29.20 mmol) were dissolved in acetonitrile (15 mL) in the presence of piperidine (0.5 mL) and then refluxed for 8 h. The solvent was removed by rotary evaporation; the residue was purified by column chromatography using silica gel (CH_2Cl_2/MeOH = 10/1) to give a red solid of 78 mg (Yield 63%). ^{1}H NMR (400 MHz, DMSO-d_6, ppm): δ 8.22 (s, 1H), 7.77 (d, J = 3.6 Hz, 1H), 7.51 (s, 1H), 7.48 (d, J = 3.6 Hz, 1H), 7.41 (d, J = 8.0 Hz, 1H), 7.21 (m, 4H), 6.83 (d, J = 8.4 Hz, 1H), 4.91 (m, 1H), 3.85 (m, 1H), 2.29 (s, 3H), 2.05 (m, 1H), 1.77 (m, 3H), 1.62 (m, 1H), 1.40 (m, 1H). ^{13}C NMR (100 MHz, DMSO-d_6, ppm): δ 164.70, 151.72, 148.35, 142.80, 138.97, 138.33, 135.79, 133.06, 131.39, 129.80, 125.95, 122.66, 122.31, 121.91, 120.10, 118.66, 106.87, 68.39, 44.29, 34.90, 32.89, 23.90, 20.38. HRMS (ESI, m/z): $[M + Na]^+$ calcd for $C_{26}H_{22}N_2NaO_2S$, 449.1300; found, 449.1303.

Synthesis of 3. A solution of *n*-butyllithium (2.5 M in hexane, 1.68 mL, 4.20 mmol) was added dropwise to a solution of bromo-substituted indoline **1** (1.16 g, 3.53 mmol) in 25 mL of predried THF at −78 °C under a nitrogen atmosphere; $B(OCH_3)_3$ (0.47 mL, 4.14 mmol) was added after the mixture was stirred at −78 °C for 1 h. The reaction mixture was allowed to warm up to room temperature 1 h later and stirred overnight. Without further purification, the mixture is used for Suzuki cross-coupling. *N*-octyl-4,7-Dibromophthalimide (1.48 g, 3.55 mmol), K_2CO_3 (2 M, 10 mL), $Pd(PPh_3)_4$ (100 mg, 0.09 mmol), and THF (30 mL) were heated to 80–90 °C under a nitrogen atmosphere for 30 min. Borate ester synthesized previously was added slowly and refluxed for a further 12 h. After cooling to room temperature, the mixture was extracted with CH_2Cl_2 (50 mL × 3). The organic portion was combined, and the solvent was removed by rotary evaporation. The residue was purified by column chromatography using silica gel (CH_2Cl_2/petroleum ether = 1/20) to give a red oil of 804 mg (Yield 39%). ^{1}H NMR (400 MHz, $CDCl_3$, ppm): δ 7.74 (d, J = 8.4 Hz, 1H), 7.46 (d, J = 8.4 Hz, 1H), 7.31 (s, 1H), 7.22 (m, 3H), 7.16 (d, J = 8.4 Hz, 2H), 6.91 (d, J = 8.4 Hz, 1H), 4.85 (m, 1H), 3.88 (m, 1H), 3.65 (t, J = 7.2 Hz, 2H), 2.34 (s, 3H), 2.07 (m, 1H), 1.93 (m, 2H), 1.79 (m, 1H), 1.65 (m, 4H), 1.26 (m, 10H), 0.86 (t, J = 4.0 Hz, 3H). ^{13}C NMR (100 MHz, $CDCl_3$, ppm): δ 166.70, 166.29, 149.04, 141.17, 139.93, 138.27, 136.75, 134.66, 131.94, 130.27, 129.81, 129.30, 128.44, 126.04, 124.67, 120.60, 115.54, 106.63, 69.33, 45.29, 38.80, 35.20, 33.65, 31.78, 29.15, 29.13, 28.43, 26.91, 24.48, 22.62, 20.82, 14.08. HRMS (ESI, m/z): $[M + H]^+$ calcd for $C_{34}H_{38}BrN_2O_2$, 585.2117; found, 585.2121.

Synthesis of 4. Compound **3** (530 mg, 0.90 mmol), 5-formylthiophen-2-yl boronic acid (281 mg, 1.80 mmol), K_2CO_3 (2 M, 15 mL), and $Pd(PPh_3)_4$ (30 mg, 0.03 mmol) were dissolved in 30 mL of THF, and the mixture was heated to 80–90 °C under a nitrogen atmosphere to reflux for 12 h. After cooling to room temperature, the mixture was extracted with CH_2Cl_2 (50 mL × 3). The organic portion was combined and removed by rotary evaporation. The residue was purified by column chromatography using silica gel (CH_2Cl_2/petroleum ether = 5/1) to give a yellow solid of 183 mg (Yield 33%). ^{1}H NMR (400 MHz, $CDCl_3$, ppm): δ 9.95 (s, 1H), 7.80 (s, 2H), 7.74 (d, J = 8.2 Hz, 1H), 7.66 (d, J = 8.2 Hz, 1H), 7.36 (s, 1H), 7.32 (m, 1H), 7.22 (d, J = 8.4 Hz, 2H), 7.17 (d, J = 8.4 Hz, 2H), 6.94 (d, J = 8.0 Hz, 1H), 4.87 (m, 1H), 3.90 (m, 1H), 3.64 (t,

J = 7.6 Hz, 2H), 2.34 (s, 3H), 2.08 (m, 1H), 1.94 (m, 2H), 1.79 (m, 1H), 1.63 (m, 4H), 1.26 (m, 10H), 0.86 (t, J = 6.3 Hz, 3H). ^{13}C NMR (100 MHz, $CDCl_3$, ppm): δ 182.90, 167.37, 167.29, 149.16, 147.48, 144.11, 142.31, 139.89, 136.29, 136.04, 135.28, 134.68, 134.65, 132.00, 130.55, 129.82, 129.52, 129.16, 128.91, 127.87, 127.80, 126.18, 124.97, 120.65, 106.61, 69.36, 45.30, 38.23, 35.21, 33.64, 31.77, 29.16, 29.14, 28.48, 26.95, 24.49, 22.61, 20.83, 14.07. HRMS (ESI, m/z): $[M + H]^+$ calcd for $C_{39}H_{41}N_2O_3S$, 617.2838; found, 617.2836.

Synthesis of LS-2. The synthesis method resembles that of compound **LS-1**, and the compound was purified by column chromatography on silica (CH_2Cl_2/MeOH = 10/1) to give an orange solid of 122 mg (Yield 66%). ^{1}H NMR (400 MHz, DMSO-d_6, ppm): δ 8.17 (s, 1H), 7.85 (d, J = 8.2 Hz, 1H), 7.77 (d, J = 6.4 Hz, 2H), 7.73 (d, J = 8.4 Hz, 1H), 7.40 (s, 1H), 7.28–7.18 (m, 5H), 6.87 (d, J = 8.3 Hz, 1H), 4.91 (m, 1H), 3.85 (m, 1H), 3.52 (t, J = 7.2 Hz, 2H), 2.29 (s, 3H), 2.03 (m, 1H), 1.80 (m, 2H), 1.64 (t, J = 5.6 Hz, 2H), 1.54 (m, 2H), 1.45 (m, 1H), 1.23 (m, 10H), 0.83 (t, J = 6.6 Hz, 3H). ^{13}C NMR (100 MHz, DMSO-d_6, ppm): δ 166.77, 166.72, 163.24, 147.91, 142.15, 140.40, 139.50, 138.18, 135.90, 135.18, 134.86, 134.08, 130.96, 130.43, 129.77, 129.31, 128.74, 128.16, 127.51, 126.36, 125.17, 119.80, 118.95, 106.06, 68.36, 44.47, 37.40, 34.80, 33.08, 31.16, 28.49, 27.69, 26.26, 23.95, 22.37, 21.82, 20.38, 13.89. HRMS (ESI, m/z): $[M + H]^+$ calcd for $C_{42}H_{42}N_3O_4S$, 684.2896; found, 684.2899.

Fabrication of Solar Cells. All chemicals and solvents used for DSSCs fabrication were of reagent-grade quality; LiI, I_2, ethanol, and 4-*tert*-butylpyridine (4-TBP) were obtained from Acros and used without further purification. Transparent TiO_2 paste was composed of nanoparticles with diameter of 15 nm, while light-scattering anatase particles were composed of a mixture of nanoparticles with diameter of 15 nm (60%) and large particles with diameter of 100 nm (40%). The pretreatment of transparent conducting oxide (TCO) glass and fabrication of solar cells were performed according to the published procedures.[6b] To scrutinize and optimize the concentration of CDCA, TiO_2 films were immersed in CDCA ethanol solution for 6 h before dipped into dye CH_2Cl_2 solution. DSSCs were fabricated using **LS-1**, **LS-2**, and **WS-5** as sensitizers with an effective working area of 0.25 cm^2, dye adsorbed TiO_2 films pasted onto TCO glass as the working electrode, Pt coated TCO glass as the counter electrode, and 0.05 M I_2, 0.10 M LiI, 0.60 M PMII, and 0.50 M 4-TBP in cosolvent of acetonitrile and methoxypropionitrile (volume ratio, 7:3) mixture solution as the redox electrolyte.

Photovoltaic Measurements. Photovoltaic measurements employed an AM 1.5 solar simulator equipped with a 300 W xenon lamp (model no. 91160, Oriel). The power of the simulated light was calibrated to 100 mW cm^{-2} using a Newport Oriel PV reference cell system (model 91150 V). Photocurrent density–voltage (I–V) curves were obtained by applying an external bias to the cell and measuring the generated photocurrent with a model 2400 source meter (Keithley Instruments, Inc. USA). The voltage step and delay time of the photocurrent were 10 mV and 40 ms, respectively. The cell active area was tested with a mask of 0.25 cm^2 with 9 μm transparent TiO_2 and 8 μm scattering TiO_2. The photocurrent action spectra were measured with the incident monochromatic photon-to-current conversion efficiency (IPCE) test system consisting of a model SR830 DSP Lock-In Amplifier and model SR540 Optical Chopper (Stanford Research Corporation, USA), a 7IL/PX150 xenon lamp and power supply and a 7ISW301 spectrometer. Electrochemical impedance spectroscopy (EIS) Nyquist and Bode plot for DSSCs was performed using a two-electrode system under dark. The spectra were scanned in a frequency range of 0.1 Hz–100 kHz at room temperature with applied bias potential set at −750 mV. The alternate current (AC) amplitude was set at 10 mV.

RESULTS AND DISCUSSION

Design and Synthesis. Phthalimide and benzotriazole polymers have been widely investigated in organic electronics due to their excellent electron transporting ability, good environmental stability, and easy solubility modification by introducing functional groups to the nitrogen site.[10,11] As shown in Figure 1, we incorporated the two moieties into the novel D-A-π-A configuration to afford the sensitizers **LS-2** and

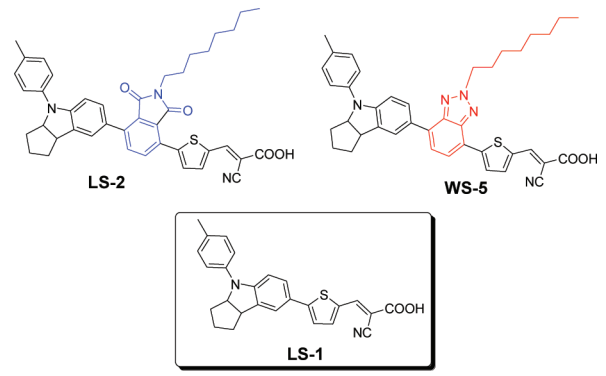

Figure 1. Chemical structures of sensitizers **LS-2** and **WS-5** and reference dye **LS-1**.

WS-5 based on the following considerations: (i) both phthalimide and benzotriazole units show high electron-affinity property; (ii) the solubilizing octyl group on *N*-position in both units can efficiently inhibit electron recombination between the oxidized species and injection electrons on the surface of TiO_2 film; and (iii) their similar structures of five-member benzoheterocycles afford a systematical comparison in photophysical and electrochemical as well as photovoltaic properties in nanocrystalline TiO_2-based DSSCs.

As illustrated in Scheme 1, the target dye **LS-2** was conveniently prepared by traditional Suzuki cross-coupling

Scheme 1. Synthetic Routes of LS-1 and LS-2[a]

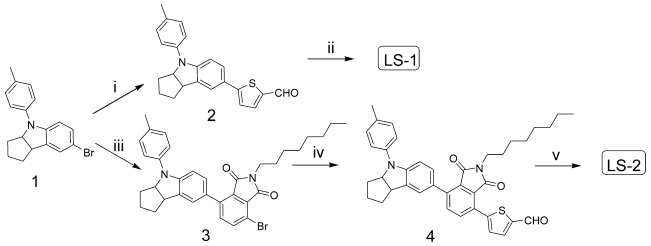

[a](i) 5-formylthiophen-2-yl boronic acid, THF, K_2CO_3, $Pd(PPh_3)_4$, reflux for 12 h, yield 41%; (ii) cyanoacetic acid, piperidine, acetonitrile, reflux for 8 h, yield 63%; (iii) (a) THF, *n*-BuLi, $B(OCH_3)_3$, (b) THF, K_2CO_3, $Pd(PPh_3)_4$, reflux for 12 h, yield 39%; (iv) 5-formylthiophen-2-yl boronic acid, THF, K_2CO_3, $Pd(PPh_3)_4$, reflux for 12 h, yield 33%; (v) cyanoacetic acid, piperidine, acetonitrile, reflux for 8 h, yield 66%.

reaction and Knoevenagel condensation reaction. **LS-1** was synthesized as reference dye based on the traditional D-π-A configuration. The synthetic routes of sensitizer **WS-5** has been reported before.[5b] **LS-1** was obtained through Suzuki coupling reaction between bromo-substituted indoline and 5-formylthiophen-2-ylboronic acid using $Pd(PPh_3)_4$ as a catalyst, followed by treatment with cyanoacetic acid in the presence of piperidine as a catalyst in acetonitrile. While for **LS-2**, two steps of Suzuki coupling reactions on *N*-octylphthalimide unit resulted in the corresponding aldehyde precursor, which was finally converted to the target dye through Knoevenagel condensation. Their chemical structures were fully characterized by ^{1}H NMR, ^{13}C NMR, and HRMS in the Experimental Section.

Photophysical and Electrochemical Properties. The UV−vis absorption spectra of dyes **LS-1**, **LS-2**, and **WS-5** in CH_2Cl_2 and on 2 μm transparent TiO_2 films are shown in Figure 2, and the corresponding data are summarized in Table 1. As a typical D-π-A or D-A-π-A system, they all exhibit a typical, strong absorption in the range of 400−600 nm with a molar extinction (ε = 1.79−2.01 × 10^4 M^{-1} cm^{-1}), which can be ascribed to the ICT process between the indoline donor part and the cyanoacetic acid acceptor moiety. To be mentioned, **LS-2** and **WS-5** exhibit an additional absorption peak around 300−400 nm. Compared with the reference compound **LS-1**, the maximum absorption peak of **WS-5** is red-shifted by 13 nm due to the incorporation of benzotriazole, which enhances the extent of electron delocalization over the whole molecule. In contrast with **LS-1**, unexpectedly, the absorption spectrum of **LS-2** with phthalimide as auxiliary acceptor shows an abnormal phenomenon with a significant blue-shift by almost 40 nm. Moreover, in **WS-5**, the additional absorption band appearing at 396 nm and the apparent red-shift in the absorption threshold are beneficial to the light harvesting. While in **LS-2**, the additional absorption band is mainly located at the ultraviolet region. That is, the two auxiliary acceptors of phthalimide and benzotriazole have a different effect on optical properties in the developed D-A-π-A featured sensitizers.

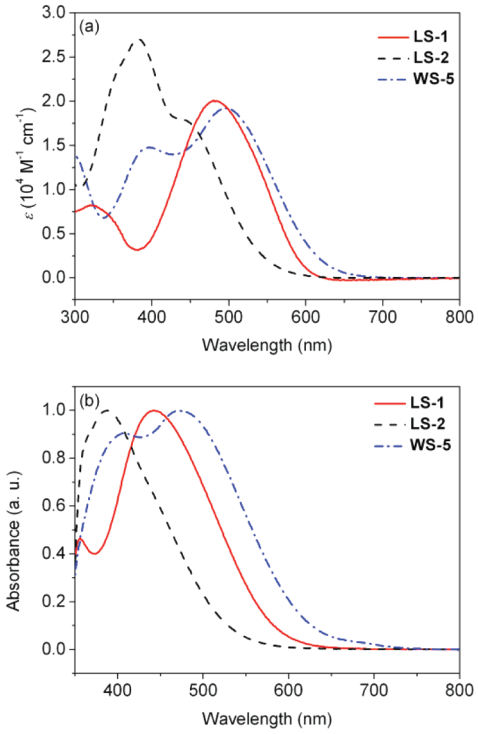

Figure 2. Absorption spectra of **LS-1**, **LS-2**, and **WS-5** measured in CH_2Cl_2 (a) and on 2 μm transparent TiO_2 films (b).

Moreover, when adsorbed onto 2 μm TiO_2 films (Table 1), the absorption peaks for **LS-1**, **LS-2**, and **WS-5** are blue-shifted to some different extent located at 442, 389, and 471 nm, respectively. Obviously, **LS-1** and **LS-2** exhibit sharp absorption hypsochromic-shift by 41 and 53 nm, respectively, while in **WS-5**, it is slightly blue-shifted by 25 nm (Figure 2b). As is well-known, when sensitizers anchored onto the nanocrystalline TiO_2 surface, the deprotonation and *H*-aggregates always result in blue-shift.[12] To study the aggregation effect on the absorption spectra, another set of TiO_2 films were stained by dye/CDCA mixtures with different dye/CDCA ratios (shown in Figure S16 in Supporting Information). As the concentration of CDCA increased in the dye bath, the absorption band of **LS-1** on TiO_2 film showed significantly red-shift, while no obvious change was observed for **LS-2**. That is, the blue-shift of **LS-2** in absorption spectra after adsorption on TiO_2 film might be predominated by deprotonation, which decreases the strength of the electron acceptor. While for **LS-1**, the phenomenon may arise by the synergy of deprotonation and aggregation effects. By comparison of absorption spectra on TiO_2 films of **LS-2** and **WS-5**, we could find that the incorporation of benzotriazole unit in **WS-5** is beneficial to countervail the deprotonation effect and contributes to the observed small blue-shift. Furthermore, due to the very large blue shift by 53 nm, the absorption band of **LS-2** is mostly shifted to below 400 nm, that is, in ultraviolet region (Figure 2b). Apparently, the absorption range of **WS-5** on TiO_2 film becomes much broader than that of **LS-1** and **LS-2** because the former shows the smallest blue-shift after adsorption. With the very similar structure, the two D-A-π-A dyes **LS-2** and **WS-5** show distinctly different variations in absorption spectra when they were adsorbed on the TiO_2 films. Therefore, it is essential to choose proper subsidiary withdrawing unit in D-A-π-A configuration.

To evaluate the possibility of electron injection and dye regeneration, cyclic voltammograms were performed in CH_2Cl_2 solution (shown in Figure 3a) with ferrocene (0.4 V vs. normal hydrogen electrode (NHE)) as external reference to determine the redox potential. The HOMO and LUMO levels of these dyes were summarized in Table 1. The first oxidation potentials of the dyes (0.66, 0.71, and 0.61 V for **LS-1**, **LS-2**, and **WS-5**, respectively), corresponding to HOMO values, are more positive than that of I_3^-/I^-, ensuring the thermodynamic regeneration of dyes. As estimated from the band gap derived from the wavelength at 10% maximum absorption intensity of these dyes adsorbed onto TiO_2 films, the resulting E_{0-0} is 2.17,

Table 1. Photophysical and Electrochemical Properties of Sensitizers LS-1, LS-2, and WS-5 in CH_2Cl_2 Solution and Adsorbed on TiO_2 Films

	absorption				
dyes	λ_{max}[a]/nm in CH_2Cl_2 (ε/M^{-1} cm^{-1})	λ_{max}[b]/nm on TiO_2	HOMO[c] (V) (vs NHE)	E_{0-0}[d] (V)	LUMO[e] (V) (vs NHE)
LS-1	483 (20100)	442	0.66	2.17	−1.51
LS-2	383 (27000) 442 (17900)	389	0.71	2.30	−1.59
WS-5	396 (14700) 496 (19200)	471	0.61	2.12	−1.51

[a]Absorption peaks (λ_{max}) and molar extinction coefficients (ε) were measured in CH_2Cl_2. [b]Absorption peaks (λ_{max}) were obtained with adsorption onto 2 μm nanocrystalline TiO_2 film deposited on TCO glass. [c]The HOMO was obtained in CH_2Cl_2 with ferrocene (0.4 V vs. NHE) as external reference. [d]E_{0-0} was derived from the wavelength at 10% maximum absorption intensity for the dye-loaded 2 μm nanocrystalline TiO_2 film. [e]The LUMO was calculated with the equation of LUMO = HOMO − E_{0-0}.

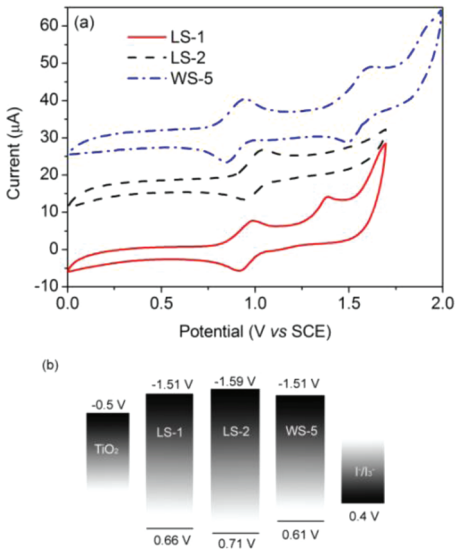

Figure 3. (a) Oxidative cyclic voltammetry plots of **LS-1**, **LS-2**, and **WS-5**. (b) Schematic diagram of energy levels of TiO_2 conduction band, dyes, and I^-/I_3^- redox couple.

2.30, and 2.12 eV for **LS-1**, **LS-2**, and **WS-5**, respectively (Table 1). Consequently, all the LUMO values of these dyes (−1.51, −1.59, and −1.51 V, respectively) are more negative than the conduction band (E_{CB}) of TiO_2, indicating the electron injection process from the LUMO orbital of these sensitizers to the conduction band of TiO_2 energetically permitted. Notably, comparing with **LS-1**, the incorporation of the benzotriazole group in **WS-5** does not have an effect on the LUMO orbital but only shifts the oxidation potential (HOMO) cathodically by 0.05 V (Figure 3b), indicating the beneficial charge transfer from donor (indoline unit) to acceptor (cyanoacetic acid) with the incorporated strong electron-withdrawing unit of benzotriazole. However, the incorporation of phthalimide unit has an effect on both HOMO and LUMO values, that is, **LS-2** shows a more positive HOMO level by 0.05 V and a more negative LUMO level by −0.08 V than that of **LS-1** (Figure 3b). Consequently, in contrast with the beneficial charge transfer of benzotriazole, the phthalimide unit in **LS-2** plays an opposite negative contribution to the charge transfer, that is, blocking ICT from donor to acceptor to some extent.

Theoretical Approach. To get insight into the effect of different additional withdrawing units of phthalimide and benzotriazole on absorption of **LS-2** and **WS-5**, the ground-state geometries, electron distribution for the frontier molecular orbitals and electronic transitions upon photo excitation were calculated by DFT and TDDFT calculations with the Gaussian09 package.[13] The ground-state geometries of these dyes have been optimized in the gas phase by DFT,[13] using the hybrid B3LYP[14] functional and the standard 6-31G(d) basis set. For the TDDFT calculations, performed on the B3LYP optimized ground-state geometries, the Coulomb attenuating B3LYP (CAM-B3LYP) approach[15] was used with 6-31+G(d) basis set. Solvation effect was taken into account into the TDDFT calculations in CH_2Cl_2 with the nonequilibrium version of the C-PCM model[16] implemented in Gaussian09.[13] Optimized ground-state geometries and dihedral angles between main aromatic rings for the optimized structures of these dyes are shown in Figure 4 and Table 2, while the TD-DFT results and frontier molecular orbitals are shown in Table 3 and Figure 5, respectively.

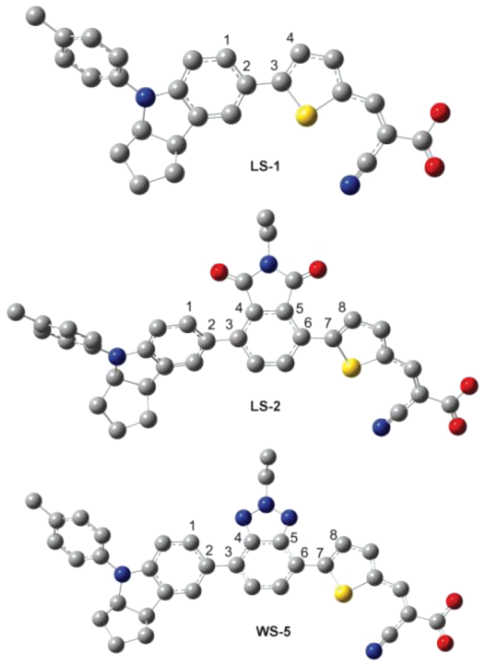

Figure 4. Optimized ground-state geometries for **LS-1**, **LS-2**, and **WS-5**. Note: the ethyl group was used instead of the octyl group in **LS-2** and **WS-5** for computational efficiency reasons.

Table 2. Critical Dihedral Angles (in Degrees) in LS-1, LS-2, and WS-5 Optimized at B3LYP/6-31G(d) Level

	|C1−C2−C3−C4|	|C5−C6−C7−C8|
LS-1	16.8	
LS-2	43.5	31.9
WS-5	26.6	0.1

Table 3. Calculated TDDFT (CAMB3LYP) Excitation Energies for the Lowest Transition (eV, nm), Oscillator Strengths (*f*), Composition in Terms of Molecular Orbital Contributions, and Experimental Absorption Maxima

dyes	state	composition[a]	*E* (eV, nm)	*f*	exp. (eV, nm)
LS-1	S1	86% H→L	2.65 (467.3)	1.3558	2.57 (483)
	S2	68% H−1→L	3.95 (313.9)	0.0814	3.98 (312)
LS-2	S1	63% H→L	2.93 (423.7)	1.1019	2.81 (442)
	S2	82% H→L+1	3.11 (398.2)	0.3341	3.24 (383)
WS-5	S1	72% H→L	2.49 (497.2)	1.6271	2.50 (496)
	S2	59% H−1→L	3.39 (365.9)	0.1511	3.13 (396)

[a]H = HOMO, L = LUMO, H−1 = HOMO−1, L+1 = LUMO+1.

As shown in Table 2, the dihedral angles formed between the donor group indoline and conjunction bridge in **LS-1** is computed to be 16.8°. For **WS-5**, the dihedral angle formed between the donor group and auxiliary acceptor benzotriazole group (|C1−C2−C3−C4|) is calculated to be 26.6°, while the angle formed between benzotriazole group and thiophene moiety (|C5−C6−C7−C8|) is calculated to be 0.1°, an exact coplanarity. It is consistent that the introduction of benzotriazole unit into the molecular frame can red-shift the ICT absorption peak by 13 nm (Table 1). Moreover, in **WS-5**, the additional absorption band appearing at 396 nm and the apparent red-shift in the absorption threshold are beneficial to the light harvesting. Consequently, the incorporated benzotriazole unit can efficiently decrease the band gap and optimize

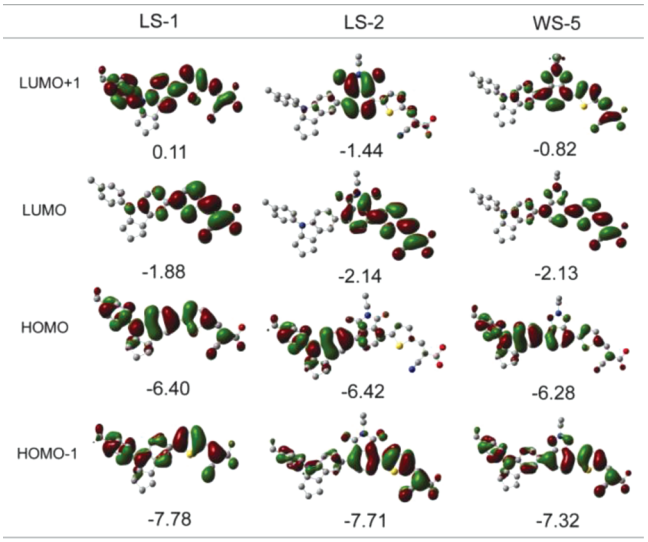

Figure 5. Calculated frontier orbitals of dyes **LS-1**, **LS-2**, and **WS-5** (isodensity = 0.020 au). Orbital Energies are in eV.

energy levels, thus resulting in broader responsive wavelength region and higher light-harvesting efficiency. In sharp contrast with **WS-5**, **LS-2** shows significant twist structure with dihedral angles formed by |C1−C2−C3−C4| and |C5−C6−C7−C8| calculated to be 43.5° and 31.9°, respectively. The twist conformation suggests that the incorporated phthalimide unit destroys electron delocalization between the donor and acceptor units, resulting in the observed distinct blue-shift in absorption. Similar phenomenon was observed in our previous work using fluorene as conjunction bridge.[6b] Generally, the aromatic rings linked by single bonds would undergo fast single bond rotation leading to coplanar conformation. However, the presence of carbonyl groups in phthalimide may interrupt the rotation of aryl groups, resulting in relatively larger dihedral angles and twist conformation. Accordingly, upon incorporation of phthalimide unit, the formed twist conformation of **LS-2** is unfavorable to electron transition from the donor part to acceptor, in accordance with a large blue shift by 41 nm in absorption spectra and more positive HOMO level (Figures 2a and 3b). Again, the deprotonation effect in **WS-5** and **LS-2** is fundamentally different due to the different conformation and coplanarity of the phthalimide and benzotriazole unit. We assume that the different hypsochromic-shift of **LS-2** and **WS-5** up adorption onto TiO_2 (Table 1) may be ascribed to their different influence on electron delocalization throughout the whole structure. Obviously, in the D-A-π-A system for **LS-2** and **WS-5**, the incorporated electron-withdrawing units of phthalimide and benzotriazole play exactly an opposite role in absorption.

As shown in Figure 5, the HOMOs for **LS-1** and **WS-5** have a π orbital delocalization throughout the entire molecule, while for **LS-2**, it is mainly localized on the donor part due to the twist structure, which would have adverse effect on electron transition from HOMO to LUMO orbital. From the analysis of the TD-DFT results in Table 3, we assign the experimental absorption band at 496 and 396 nm of **WS-5** as transitions from H→L and H−1→L. The two electronic transitions in **WS-5** are positively contributed to electron injection since both transitions correspond to electron transfer from the whole molecule (H and H−1) to the anchoring group (L), which is the main electron flux from excited dyes to the CB of semiconductor TiO_2. In contrast, the absorption bands of **LS-2** located at 442 and 383 nm are ascribed to electron transitions from H→L and H→L+1, respectively. The former corresponds to electron transfer from the indoline part to the cyanoacrylic acid segment, while the later arises from electron transition from the indoline to the phthalimide core, which is far from the anchoring group. Therefore, the electron flux of **LS-2** injected to the CB of semiconductor TiO_2 will be reduced.

Photovoltaic Performance. Figure 6 shows the action spectra of IPCE for DSSCs based on **LS-1**, **LS-2**, and **WS-5** as a

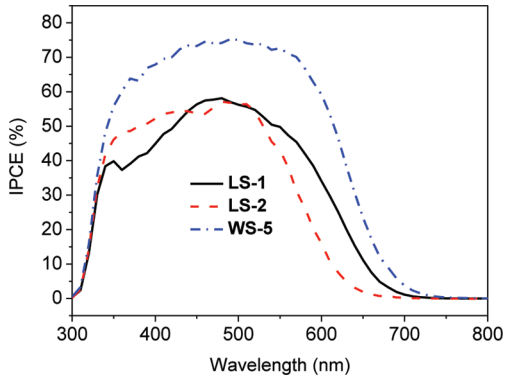

Figure 6. IPCE action spectra of DSSCs sensitized by **LS-1**, **LS-2**, and **WS-5** without coadsorption of CDCA.

function of light excitation wavelength. The IPCE onsets for **LS-1**, **LS-2**, and **WS-5** are 700, 650, and 740 nm, respectively, increasing in the order of **LS-2** < **LS-1** < **WS-5**. The IPCE of **WS-5** is higher than 70% in the range of 400−650 nm with a maximum value of 80% at 500 nm. It seems that introduction of benzotriazole in **WS-5** with good delocalization between the donor and anchoring group may broaden the spectrum of absorption to get better IPCE. Compared to **LS-1**, the IPCE data of **WS-5** is much higher, despite lower ε, indicating the incorporation of benzotriazole is beneficial to obtain the higher conversion efficiency. However, in the case of **LS-2**, the corresponding IPCE value becomes quite lower with narrow profile. Again, the IPCE spectra of **LS-2** and **WS-5** are in good consistency with their absorption spectra on the TiO_2 film (Figure 2b) and light harvesting efficiency. In the system of **WS-5** and **LS-2**, the opposite effect of five-member benzoheterocycles as auxiliary acceptor on IPCE action spectra further indicates that the modification in D-A-π-A configuration should be carried out carefully.

Figure 7 presents $I-V$ curves of the cells measured at 100 mW cm^{-2} under simulated 1.5 air mass global solar light, and parameters like J_{SC}, V_{OC}, *ff*, and η are summarized in Table 4. Compared to **LS-1**, the J_{SC} of **WS-5** was enhanced significantly from 11.25 to 15.79 mA cm^{-2}, and V_{OC} increased by 168 mV from 623 to 791 mV due to the incorporation of *n*-octyl substituted benzotriazole into the dye skeleton. However, with the similar modification, **LS-2** shows an almost unchanged photocurrent, mainly due to the disadvantageous absorption behaviors with respect to **WS-5**.

Generally, in DSSCs, CDCA is always introduced as coadsorbent to hinder strong intermolecular interaction for breaking up dye aggregation due to its steric structure.[8] To gain insight into the effect of *n*-octyl chain on the photovoltaic performance, TiO_2 films were pretreated with different concentration of CDCA in ethanol solution. As illustrated in

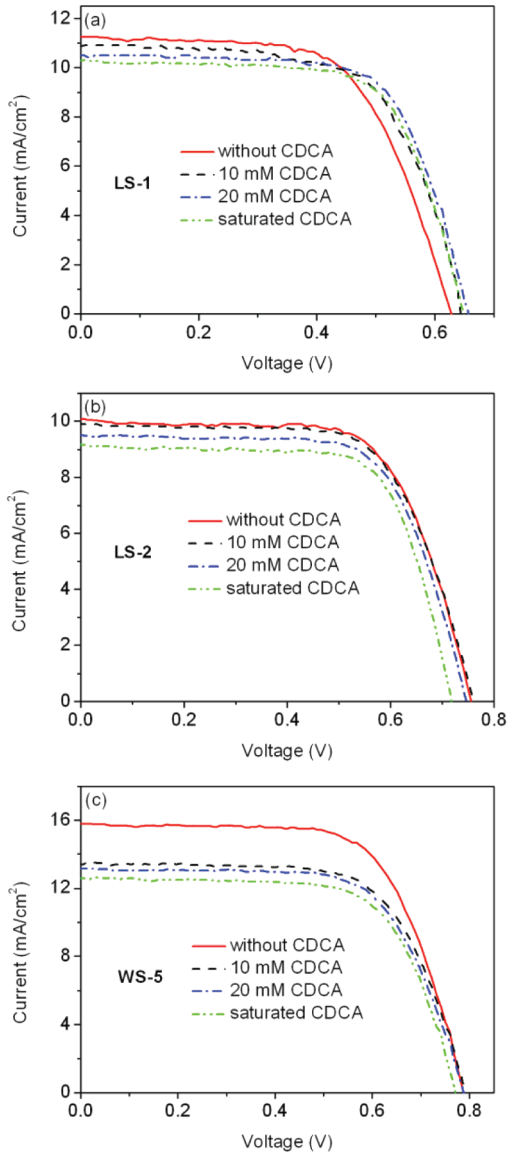

Figure 7. Photocurrent–voltage characteristics of DSSCs sensitized by **LS-1** (a), **LS-2** (b), and **WS-5** (c) coadsorbed with CDCA.

Table 4. Effect of CDCA on Photovoltaic Performances of LS-1, LS-2, and WS-5

dyes	CDCA	J_{SC}/mA cm^{-2}	V_{OC}/mV	*ff*	η/%
LS-1	0[a]	11.25	623	0.63	4.42
	10 mM[b]	10.89	649	0.65	4.59
	20 mM[c]	10.58	650	0.69	4.72
	saturated[d]	10.25	644	0.69	4.54
LS-2	0[a]	10.06	748	0.68	5.11
	10 mM[b]	9.85	753	0.68	5.04
	20 mM[c]	9.53	738	0.69	4.85
	saturated[d]	9.14	705	0.72	4.65
WS-5	0[a]	15.79	791	0.67	8.38
	10 mM[b]	13.66	796	0.66	7.12
	20 mM[c]	13.16	791	0.67	6.98
	saturated[d]	12.43	767	0.69	6.62

[a]Immersed in ethanol solution without CDCA before use. [b]Immersed in ethanol solution with 10 mM CDCA before use. [c]Immersed in ethanol solution with 20 mM CDCA before use. [d]Immersed in ethanol solution with saturated CDCA before use.

Figure 7, only **LS-1** shows significant enhancement in photovoltage coadsorbed with CDCA, while for **LS-2** and **WS-5**, there is no obvious change. In the cases of **LS-2** and **WS-5** containing a long alkyl group, the J_{SC} decreased with an incremental amount of CDCA. One possible explanation is that the coverage of dyes on TiO_2 films is decreased along with the coadsorption of CDCA, leading to a loss in the light harvest, thus decreasing current density.[9] The V_{OC} of **LS-1** increased with coadsorption of CDCA but decreased with further increasing CDCA to be saturated. When the concentration of CDCA is below 20 mM, with the increasing CDCA concentration, the V_{OC} value increased because the suppression of dye aggregation with CDCA is beneficial to extend the injection electron lifetime and inhibit charge recombination.[1a,b] However, with further increasing CDCA concentration, the V_{OC} values decreased, which may be explained as the decrease in the conduction band edge of TiO_2 semiconductor caused by excessive amounts of CDCA.[9] The best photoelectric conversion yield of **LS-1** was obtained when coadsorbed with 20 mM CDCA, while for **LS-2** and **WS-5** with *n*-octyl on the skeleton structure, a highest photoelectric conversion yield was obtained without coadsorption of CDCA, indicating that dye aggregation is efficiently prohibited by the alkyl chain. Without coadsorption of CDCA, the DSSCs based on **WS-5** exhibited a maximum solar energy to electricity conversion efficiency (η) of 8.38% with significant enhancement in all photovoltaic parameters (J_{SC} = 15.79 mA cm^{-2}, V_{OC} = 791 mV, *ff* = 0.67). However, with the very similar D-A-π-A feature changing the additional acceptor from benzotriazole to phthalimide unit, the photovoltatic efficiency based on **LS-2** was only 5.11%, decreased by 39%, with less efficient photovoltaic parameters (J_{SC} = 10.06 mA cm^{-2}, V_{OC} = 748 mV, *ff* = 0.68).

Electrochemical Impedance Spectroscopy (EIS). EIS analysis is an important method to study charge recombination and the redox reaction process at the platinum counter electrode in DSSCs in terms of equivalent circuits.[17,19] Figure 8 shows the Nyquist and Bode plots for DSSCs based on **LS-1**, **LS-2**, and **WS-5** measured under the dark. In the Nyquist diagram, three semicircles were observed in the measured frequency range of 0.1 Hz–100 kHz. The three semicircles are attributed to the reduction process of I_3^- at Pt/electrolyte interface (Z_1), charge transfer in the TiO_2/dye/electrolyte interface (Z_2), and carrier transport within electrolyte (Z_3), respectively.[18] The resistance element R_h in the high frequency range corresponds to the sheet resistance of TCO and the contact resistance between the TCO and TiO_2. In our work, EIS analysis was performed to further clarify the effect of structure modification on V_{OC}. As listed in Table 5, R_h and R_1 of three dye-based solar cells show almost the same value due to the same electrolyte and electrode in both materials and surface area. The charge transfer impedance from TiO_2 to electrolyte, R_2, corresponding to the diameter of middle-frequency semicircle of Nyquist plot, increases in the order of **LS-1** (21.63 Ohm cm^{-2}) < **LS-2** (71.34 Ohm cm^{-2}) < **WS-5** (101.4 Ohm cm^{-2}). The significant enhancement of R_2 indicates that the introduction of alkyl chains to the dyes molecules is effective in TiO_2/dye/electrolyte interface modification.

Besides, the reaction resistance of the DSSCs was analyzed by software (ZSimpWin) using an equivalent circuit shown in Figure 8c and the parameters obtained by fitting the impedance spectra shown in Table 5.[17,20] The higher V_{OC} of **LS-2** and **WS-5** can be further explained by electron lifetime, calculated

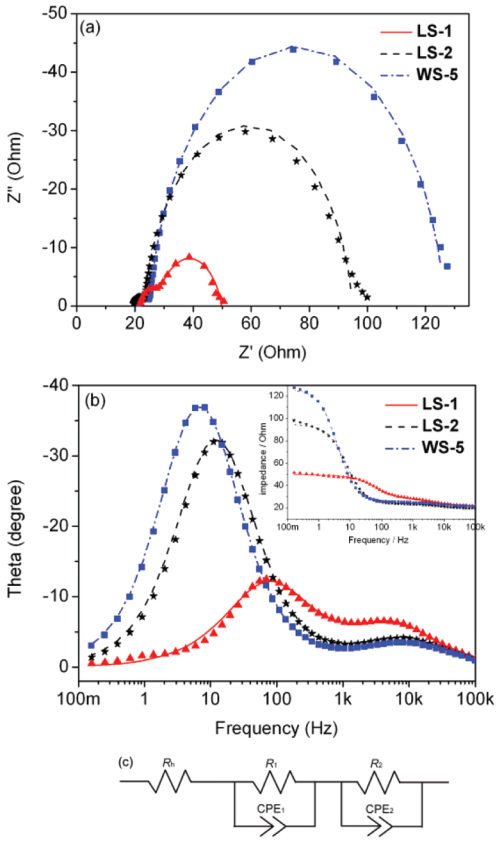

Figure 8. EIS Nyquist (a) and Bode (b) plots and equivalent circuit (c) for DSSCs based on **LS-1**, **LS-2**, and **WS-5** measured under the dark. The lines of (a) and (b) show theoretical fits using the equivalent circuits (c).

Table 5. Parameters Obtained by Fitting the Impedance Spectra of the DSSCs with LS-1, LS-2, and WS-5 Sensitizers Using the Equivalent Circuit (Figure 8c)[a]

cells	LS-1	LS-2	WS-5
R_h/Ohm cm^{-2}	21.81	19.30	21.11
CPE$_1$/μF cm^{-2}	31.4	51.3	83.6
n_1	0.8205	0.7914	0.7450
R_1/Ohm cm^{-2}	6.36	4.10	4.05
CPE$_2$/μF cm^{-2}	424	558	707
n_2	0.8080	0.9076	0.9161
R_2/Ohm cm^{-2}	21.63	71.34	101.4
τ_e/ms	2.9	14.4	54.0

[a]Equivalent circuit of the DSSC consisting of TiO$_2$/dye/electrolyte and Pt/electrolyte interface; R_h, R_1, and R_2 are the series resistance of Pt and TCO, charge transfer resistance at Pt/electrolyte, and at TiO$_2$/dye/electrolyte interface, respectively; CPE$_1$ and CPE$_2$ are the constant phase element for the TiO$_2$/dye/electrolyte and Pt/electrolyte interface, respectively. n presents the degree of surface inhomogeneity; τ_e is calculated from the relation $\tau_e = 1/(2\pi f)$.

through the relation $\tau_e = 1/(2\pi f)$ (f is the peak frequency of charge transfer in Z_2 in EIS Bode plot). For the three devices, the peak frequency decreased in the order of **LS-1** > **LS-2** > **WS-5**, and the electron lifetime was enhanced in reverse with the calculated values of 2.9, 14.4, and 54.0 ms, respectively. The longer electron lifetime of **LS-2** and **WS-5** explained the significant enhancement in V_{OC} for **LS-2** and **WS-5** in $I-V$ test (Table 4). Here, comparing the additional acceptor contribution in D-A-π-A feature, the benzotriazole and phthalimide units can increase electron lifetime by 18.6- and 5.0-fold, respectively, with respect to **LS-1**. Again, the distinctly longer electron lifetime of **WS-5** with respect to **LS-2** is further indicative of the vital effect of subsidiary withdrawing unit in D-A-π-A configuration.

CONCLUSIONS

In summary, we have developed two novel D-A-π-A organic dyes **LS-2** and **WS-5** by incorporating phthalimide and benzotriazole as the additional electron-withdrawing units based on the following considerations: (i) both the two units show high electron-affinity property; (ii) the *N*-position in both units supply conveniently a modification position for solubilizing alkyl chains, which can efficiently inhibit electron recombination between the oxidized species and inject electrons on the surface of TiO$_2$ film; (iii) their similar five-member benzo-heterocycles structures afford a systematical comparison investigations in choice of the auxiliary acceptors in D-A-π-A dyes. Our results indicate that the two auxiliary acceptors play exactly different roles in affecting the absorption and electrochemical properties of the D-A-π-A dyes. Compared with reference dye **LS-1**, the absorption spectra of **WS-5** show distinctly batho-chromic shift both in CH_2Cl_2 and on TiO$_2$ film due to the incorporation of benzotriazole. However, the phthalimide in **LS-2** shows a negative effect on extending the absorption range due to the twist conformation formed between phthalimide and its neighboring groups, resulting in significant hypso-chromic shift in absorption spectra of **LS-2**. The molecular simulation on the two dyes indicates that the benzotriazole unit facilitates the orbital overlap between HOMO and LUMO. While the twist structure around the phthalimide unit, conversely, breaks the molecular conjugation, which is unfavorable to the charge migration from donor to acceptor. Due to the existence of alkyl chain, both of the two dyes show preferable photovoltaic performance with considerable high photovoltage (>750 mV) even without CDCA treatment. The conversion efficiency for **WS-5**-based DSSCs achieves 8.31%, which is 64% higher than that of **LS-2** mainly due to its better photocurrent. EIS measurements further indicated that, with respect to octyl-phthalimide, the incorporation of octyl-benzotriazole is more favorable to TiO$_2$/dye/electrolyte interface modification and injected electron lifetime enhancement. The large difference between **WS-5** and **LS-2** in absorption, energy levels, and photovoltaic performances caused by the additional electron-withdrawing units indicates that the auxiliary acceptor unit in the D-A-π-A configuration dyes should be screened with caution.

ASSOCIATED CONTENT

Supporting Information

^{1}H NMR, ^{13}C NMR, and HRMS spectra of intermediates, **LS-1** and **LS-2**, and absorption spectra of **LS-1** and **LS-2** coadsorbed with different amounts of CDCA. This material is available free of charge via the Internet at http://pubs.acs.org.

AUTHOR INFORMATION

Corresponding Author

*Fax: (+86) 21-6425-2758. E-mail: whzhu@ecust.edu.cn.

Notes

The authors declare no competing financial interest.

■ ACKNOWLEDGMENTS

This work was financially supported by NSFC/China, National 973 Program (2011CB808400), the Oriental Scholarship, SRFDP 200802510011, the Fundamental Research Funds for the Central Universities (WK1013002), and STCSM (10dz2220500).

■ REFERENCES

(1) (a) Hagfeldt, A.; Boschloo, G.; Sun, L. C.; Kloo, L.; Pettersson, H. *Chem. Rev.* **2010**, *110*, 6595−6663. (b) Mishra, A.; Fischer, M. K. R.; Bäuerle, P. *Angew. Chem., Int. Ed.* **2009**, *48*, 2474−2499. (c) Ooyama, Y.; Harima, Y. *Eur. J. Org. Chem.* **2009**, 2903−2934. (d) Li, C.; Yum, J. H.; Moon, S. J.; Herrmann, A.; Eickemeyer, F.; Pschirer, N. G.; Erk, P.; Schöneboom, J.; Müllen, K.; Grätzel, M.; Nazeeruddin, M. K. *ChemSusChem* **2008**, *1*, 615−618. (e) Qin, H.; Wenger, S.; Xu, M.; Gao, F.; Jing, X.; Wang, P.; Zakeeruddin, S. M.; Grätzel, M. *J. Am. Chem. Soc.* **2008**, *130*, 9202−9203. (f) Zhang, X. H.; Wang, Z. S.; Cui, Y.; Koumura, N.; Furube, A.; Hara, K. *J. Phys. Chem. C* **2009**, *113*, 13409−13415. (g) Jeon, S.; Jo, Y.; Kim, K. J.; Jun, Y.; Han, C. H. *ACS Appl. Mater. Interfaces* **2011**, *3*, 512−516. (h) Zeng, W. D.; Cao, Y. M.; Bai, Y.; Wang, Y. H.; Shi, Y. S.; Zhang, M.; Wang, F. F.; Pan, C. Y.; Wang, P. *Chem. Mater.* **2010**, *22*, 1915−1925. (i) Tian, H. N.; Yu, Z.; Hagfeldt, A.; Kloo, L.; Sun, L. C. *J. Am. Chem. Soc.* **2011**, *133*, 9413−9422. (j) Chiba, Y.; Islam, A.; Watanabe, Y.; Komiya, R.; Koide, N.; Han, L. Y. *Jpn. J. Appl. Phys. Part 2* **2006**, *45*, L638−L640. (k) Dias, F. B.; King, S.; Monkman, A. P.; Perepichka, I. I.; Kryuchkov, M. A.; Perepichka, I. F.; Bryce, M. R. *J. Phys. Chem. B* **2008**, *112*, 6557−6566. (l) Nayak, P. K.; Bisquert, J.; Cahen, D. *Adv. Mater.* **2011**, *23*, 2870−2876. (m) Calogero, G.; Di Marco, G.; Cazzanti, S.; Caramori, S.; Argazzi, R.; Bignozzi, C. A. *Energy Environ. Sci.* **2009**, *2*, 1162−1172.

(2) Yella, A.; Lee, H. W.; Tsao, H. N.; Yi, C. Y.; Chandiran, A. K.; Nazeeruddin, M. K.; Diau, E. W. G.; Yeh, C. Y.; Zakeeruddin, S. M.; Grätzel, M. *Science* **2011**, *334*, 629−634.

(3) (a) Li, G.; Zhou, Y. F.; Cao, X. B.; Bao, P.; Jiang, K. J.; Lin, Y.; Yang, L. M. *Chem. Commun.* **2009**, 2201−2203. (b) Im, H.; Kim, S.; Park, C.; Jang, S. H.; Kim, C. J.; Kim, K.; Park, N. G.; Kim, C. *Chem. Commun.* **2010**, *46*, 1335−1337. (c) Zhang, M.; Liu, J. Y.; Wang, Y. H.; Zhou, D. F.; Wang, P. *Chem. Sci.* **2011**, *2*, 1401−1406. (d) Teng, C.; Yang, X. C.; Li, S. F.; Cheng, M.; Hagfeldt, A.; Wu, L. Z.; Sun, L. C. *Chem.—Eur. J.* **2010**, *16*, 13127−13138. (e) Xu, M. F.; Li, R. Z.; Pootrakulchote, N.; Shi, D.; Guo, J.; Yi, Z. H.; Zakeeruddin, S. M.; Grätzel, M.; Wang, P. *J. Phys. Chem. C* **2008**, *112*, 19770−19776.

(4) (a) Wei, D. *Int. J. Mol. Sci.* **2010**, *11*, 1103−1113. (b) Ning, Z. J.; Fu, Y.; Tian, H. *Energy Environ. Sci.* **2010**, *3*, 1170−1181. (c) Cao, Y. M.; Bai, Y.; Yu, Q. J.; Cheng, Y. M.; Liu, S.; Shi, D.; Gao, F. F.; Wang, P. *J. Phys. Chem. C* **2009**, *113*, 6290−6297. (d) Teng, C.; Yang, X. C.; Yang, C.; Li, S. F.; Cheng, M.; Hagfeldt, A.; Sun, L. C. *J. Phys. Chem. C* **2010**, *114*, 9101−9110. (e) Listorti, A.; O'Regan, B.; Durrant, J. R. *Chem. Mater.* **2011**, *23*, 3381−3399.

(5) (a) Zhu, W. H.; Wu, Y. Z.; Wang, S. T.; Li, W. Q.; Li, X.; Chen, J.; Wang, Z. S.; Tian, H. *Adv. Funct. Mater.* **2011**, *21*, 756−763. (b) Cui, Y.; Wu, Y. Z.; Lu, X. F.; Zhang, X.; Zhou, G.; Miapeh, F. B.; Zhu, W. H.; Wang, Z. S. *Chem. Mater.* **2011**, *23*, 4394−4401. (c) Wu, Y. Z.; Zhang, X.; Li, W. Q.; Wang, Z. S.; Tian, H.; Zhu, W. H. *Adv. Energy Mater.* **2012**, *2*, 149−156.

(6) (a) Liu, B.; Zhu, W. H.; Zhang, Q.; Wu, W. J.; Xu, M.; Ning, Z. J.; Xie, Y. S.; Tian, H. *Chem. Commun.* **2009**, 1766−1768. (b) Li, W. Q.; Wu, Y. Z.; Li, X.; Xie, Y. S.; Zhu, W. H. *Energy Environ. Sci.* **2011**, *4*, 1830−1837.

(7) (a) Karlsson, K. M.; Jiang, X.; Eriksson, S. K.; Gabrielsson, E.; Rensmo, H.; Hagfeldt, A.; Sun, L. C. *Chem.—Eur. J.* **2011**, *17*, 6415−6424. (b) Li, G.; Jiang, K. J.; Bao, P.; Li, Y. F.; Li, S. L.; Yang, L. M. *New J. Chem.* **2009**, *33*, 868−876. (c) Demeter, D.; Rousseau, T.; Leriche, P.; Cauchy, T.; Po, R; Roncali, J. *Adv. Funct. Mater.* **2011**, *21*, 4379−4387. (d) Roncali, J. *Adv. Energy Mater.* **2011**, *1*, 147−160. (e) Fan, H. J.; Zhang, M. J.; Guo, X.; Li, Y. F.; Zhan, X. W. *ACS Appl. Mater. Interfaces* **2011**, *3*, 3646−3653.

(8) (a) Mikroyannidis, J. A.; Suresh, P.; Roy, M. S.; Sharma, G. D. *Electrochim. Acta* **2011**, *56*, 5616−5623. (b) Lim, J.; Kwon, Y. S.; Park, T. *Chem. Commun.* **2011**, *47*, 4147−4149.

(9) Qu, S. Y.; Wu, W. J.; Hua, J. L.; Kong, C.; Long, Y. T.; Tian, H. *J. Phys. Chem. C* **2010**, *114*, 1343−1349.

(10) (a) Lee, J. Y.; Song, K. W.; Ku, J. R.; Sung, T. H.; Moon, D. K. *Sol. Energy Mater. Sol. Cells* **2011**, *95*, 3377−3384. (b) Guo, X. G.; Kim, F. S.; Jenekhe, S. A.; Watson, M. D. *J. Am. Chem. Soc.* **2009**, *131*, 7206−7207.

(11) (a) Zhang, L. J.; He, C.; Chen, J. W.; Yuan, P.; Huang, L.; Zhang, C.; Cai, W. Z.; Liu, Z. T.; Cao, Y. *Macromolecules* **2010**, *43*, 9771−9778. (b) Li, C.; Liu, M. Y.; Pschirer, N. G.; Baumgarten, M.; Müllen, K. *Chem. Rev.* **2010**, *110*, 6817−6855.

(12) (a) Chen, R. K.; Yang, X. C.; Tian, H. N.; Sun, L. C. *Photochem. Photobiol., A: Chem.* **2007**, *189*, 295−300. (b) Lin, L. Y.; Tsai, C. H.; Wong, K. T.; Huang, T. W.; Hsieh, L.; Liu, S. H.; Lin, H. W.; Wu, C. C.; Chou, S. H.; Chen, S. H.; Tsai, A. I. *J. Org. Chem.* **2010**, *75*, 4778−4785.

(13) Frisch, M. J.; Trucks, G. W.; Schlegel, H. B.; Scuseria, G. E.; Robb, M. A.; Cheeseman, J. R.; Scalmani, G.; Barone, V.; Mennucci, B.; Petersson, G. A.; Nakatsuji, H.; Caricato, M.; Li, X.; Hratchian, H. P.; Izmaylov, A. F.; Bloino, J.; Zheng, G.; Sonnenberg, J. L.; Hada, M.; Ehara, M.; Toyota, K.; Fukuda, R.; Hasegawa, J.; Ishida, M.; Nakajima, T.; Honda, Y.; Kitao, O.; Nakai, H.; Vreven, T.; Montgomery, J. A.; Peralta, J. E.; Ogliaro, F.; Bearpark, M.; Heyd, J. J.; Brothers, E.; Kudin, K. N.; Staroverov, V. N.; Kobayashi, R.; Normand, J.; Raghavachari, K.; Rendell, A.; Burant, J. C.; Iyengar, S. S.; Tomasi, J.; Cossi, M.; Rega, N.; Millam, J. M.; Klene, M.; Knox, J. E.; Cross, J. B.; Bakken, V.; Adamo, C.; Jaramillo, J.; Gomperts, R.; Stratmann, R. E.; Yazyev, O.; Austin, A. J.; Cammi, R.; Pomelli, C.; Ochterski, J. W.; Martin, R. L.; Morokuma, K.; Zakrzewski, V. G.; Voth, G. A.; Salvador, P.; Dannenberg, J. J.; Dapprich, S.; Daniels, A. D.; Farkas, O.; Foresman, J. B.; Ortiz, J. V.; Cioslowski, J.; Fox, D. J. *Gaussian 09, Revision A.02*; Gaussian, Inc.: Wallingford CT, 2009.

(14) Becke, A. D. *J. Chem. Phys.* **1993**, *98*, 1372−1377.

(15) Yanai, T.; Tew, D. P.; Handy, N. C. *Chem. Phys. Lett.* **2004**, *393*, 51−57.

(16) Cossi, M.; Barone, V. *J. Chem. Phys.* **2001**, *115*, 4708−4717.

(17) Longo, C.; Nogueira, A. F.; De Paoli, M. A.; Cachet, H. *J. Phys. Chem. B* **2002**, *106*, 5925−5930.

(18) (a) Koide, N.; Islam, A.; Chiba, Y.; Han, L. *J. Photochem. Photobiol., A: Chem.* **2006**, *182*, 296−305. (b) Wagner, K.; Griffith, M. J.; James, M.; Mozer, A. J.; Wagner, P.; Triani, G.; Officer, D. L.; Wallace, G. G. *J. Phys. Chem. C* **2010**, *115*, 317−326.

(19) Barsoukov, E.; Macdonald, J. R. *Impedance Spectroscopy Theory, Experiment, and Applications*, 2nd ed.; Wiley-Interscience: Hoboken, NJ, 2005.

(20) Wu, W.; Xu, X.; Yang, H.; Hua, J.; Zhang, X.; Zhang, L.; Long, Y.; Tian, H. *J. Mater. Chem.* **2011**, *21*, 10666−10671.